Transonic Potential Flow around Axisymmetric Inlets and Bodies at Angle of Attack

T. A. Reyhner*
Boeing Commercial Airplane Company, Seattle, Wash.

An analysis has been developed and a computer program written to predict transonic potential flow about axisymmetric inlets, with or without centerbodies, and axisymmetric bodies at an arbitrary angle of attack. The method is a line relaxation solution of the complete potential flow equation in a cylindrical coordinate system. The only restriction of the program is that the body be axisymmetric; the computer flowfield is fully three-dimensional. Special differencing is used for θ derivatives in order to reduce greatly the cost of computation by allowing the use of coarse mesh spacing in θ. Several comparisons between theory and experiment are presented to show the validity of the analysis.

Nomenclature

a = local speed of sound
D = diameter
L = inlet length, hilite to compressor face
M = Mach number
M_{TH} = average (one-dimensional) throat Mach number
n = coordinate normal to surface
$\boldsymbol{n}$ = unit normal to surface
q = velocity, $(u^2+v^2+w^2)^{1/2}$
r = radius
Δr = mesh spacing in r
u = component of velocity along x coordinate
u_r = radial component of velocity
u_θ = circumferential component of velocity
v = component of velocity along y coordinate
w = axial component of velocity
x = coordinate, $r\cos\theta$
y = coordinate, $r\sin\theta$
z = axial coordinate
Δz = mesh spacing in z
γ = ratio of specific heats
θ = circumferential coordinate
$\Delta\theta$ = mesh spacing in θ
ϕ = potential function
ϕ_n = $\partial\phi/\partial n$, velocity normal to surface
ϕ_r = $\partial\phi/\partial r = u_r$, radial velocity
ϕ_x = $\partial\phi/\partial x = u$, x velocity component
ϕ_y = $\partial\phi/\partial y = v$, y velocity component
ϕ_z = $\partial\phi/\partial z = w$, axial velocity
ϕ_1, ϕ_2 = see Eq. (12)
ω = local over-relaxation parameter
ω_n = overall (nominal) over-relaxation parameter

Superscripts

$+$ = value after updating during relaxation sweep

Subscripts

i,j,k = mesh indices, z, r, and θ, respectively
K = number of θ mesh lines, and index for the $\theta = 180°$ mesh line
$k90$ = k index for $\theta = 90°$ mesh line
ℓ, u = mesh spacing subscripts
r,z,θ = partial derivatives
x,y = partial derivatives
∞ = freestream

Received Jan. 20, 1977; presented as Paper 77-145 at the AIAA 15th Aerospace Sciences Meeting, Los Angeles, Calif., Jan. 24-26, 1977; revision received June 8, 1977.
Index categories: Aerodynamics; Transonic Flow.
*Specialist Engineer, Propulsion Technology Research. Associate Fellow AIAA.

Introduction

TECHNIQUES[1-8] are now well established for calculating solutions of the complete equations for two-dimensional and axisymmetric transonic potential flow. The problem of predicting three-dimensional flow is more difficult. As a consequence, solutions of the complete potential flow equation[9,10] are available only for specific geometries. The basic approach used in this work was developed to be applicable to the general three-dimensional flow problem, but at this time the programming task has been simplified greatly by restricting the body geometry to be axisymmetric. The computed flow is three dimensional.

The full equations of compressible potential flow are solved in a cylindrical coordinate system. The program will compute the transonic potential flow about an axisymmetric body or inlet, with or without centerbody, at an arbitrary angle of attack. The angle-of-attack capability includes crosswind cases (angle of attack equals 90°) and angles of attack greater than 90°, which might be encountered in an inlet for a VTOL airplane, for instance. The program will calculate the potential field for any subsonic freestream velocity; the local flow may be supersonic. The analysis will handle inlets or axisymmetric bodies of almost any shape. The primary restriction on inlet or axisymmetric body geometry is the maximum number of mesh that the computer program can use. The number of mesh lines that the computer program can use is a function of specified array storage and has been set as a result of a tradeoff study between cost of a computer run and accuracy. If an extremely complex inlet geometry is specified, accuracy will be degraded because the mesh will not be sufficiently dense to resolve all of the features of the flow.

The derivatives in the partial differential equations for potential flow are replaced with difference quotients. The resulting finite-difference equations are solved using line relaxation along radial lines. The approach is an extension of the axisymmetric work reported earlier.[1] The restriction that the geometry be axisymmetric, only effects the treatment of the boundary condition at body surfaces; the solution away from the body is not dependent on the body geometry being axisymmetric. The primary difficulties expected to be en-

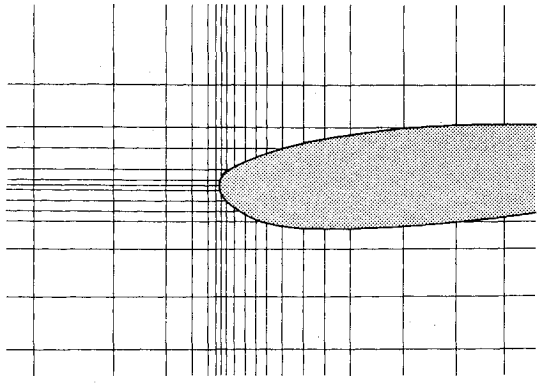

Fig. 1 Typical coarse computational mesh for a θ = constant plane in the vicinity of the hilite.

countered in an extension of this analysis to full three-dimensional geometry would be the development of coding for specifying the geometry, logic for keeping track of the surfaces, and logic for coupling the difference equations together for the line relaxation

Flow about several inlets at various angles of attack has been calculated and compared with experimental data. These comparisons indicate that the analysis does predict flow correctly where there is no boundary-layer separation. Results also are shown for an axisymmetric body at angles of attack. Considerable effort has been made to make the computer program as efficient as possible to provide a cost-effective tool for design and analysis. Also, many experimental cases have been compared to the results of the program in order to verify the analysis and to discover its limitations. It is shown that the results of the program are sufficiently accurate for both analysis and design tasks.

Approach

The full equations for compressible potential flow are solved in a cylindrical coordinate system using finite differences and line relaxation. The analysis is a direct extension of an axisymmetric-flow-analysis procedure[1] which uses a Cartesian mesh (r,z). Figure 1 shows a typical coarse computational mesh for a θ = constant plane in the vicinity of the inlet hilite (forwardmost point of the cowl). The logic and techniques of the axisymmetric analysis have been used to handle derivatives in the θ = constant planes. The requirement that the body geometry be axisymmetric makes the mesh in the r = constant and z = constant planes regular at surfaces and simplifies differencing in these planes. Special difference formulas are developed for the derivatives with respect to θ in order to make the analysis significantly more efficient. Initial relaxation is on a coarse mesh, and extrapolation of residue fields is used to speed convergence and thus minimize computational costs.

Equation

The complete equation for compressible potential flow expressed in cylindrical coordinates is

$$(a^2-\phi_r^2)\phi_{rr}+\left(a^2-\frac{\phi_\theta^2}{r^2}\right)\frac{\phi_{\theta\theta}}{r^2}+(a^2-\phi_z^2)\phi_{zz}-2\frac{\phi_r\phi_\theta}{r^2}\phi_{r\theta}$$
$$-2\phi_r\phi_z\phi_{rz}-2\frac{\phi_\theta\phi_z}{r^2}\phi_{\theta z}+\left(a^2+\frac{\phi_\theta^2}{r^2}\right)\frac{\phi_r}{r}=0 \qquad (1)$$

where

$$a^2=a_\infty^2-\frac{\gamma-1}{2}\left(\phi_r^2+\frac{\phi_\theta^2}{r^2}+\phi_z^2-q_\infty^2\right) \qquad (2)$$

The velocity components for the cylindrical coordinate system (r,θ,z) are

$$u_r=\phi_r, \quad u_\theta=\phi_\theta/r, \quad w=\phi_z \qquad (3)$$

which are related to the Cartesian mesh (x,y,z) velocity components (u,v,w) by

$$u_r=u\cos\theta+v\sin\theta \qquad (4a)$$

$$u_\theta=-u\sin\theta+v\cos\theta \qquad (4b)$$

On the axis $(r=0)$, Eq. (1) cannot be applied. Along the axis the potential equation for Cartesian coordinates is used, together with the requirement that there are θ mesh for $\theta=0°$, 90°, and 180°. The Cartesian coordinate form of the potential flow equation is

$$(a^2-\phi_x^2)\phi_{xx}+(a^2-\phi_y^2)\phi_{yy}+(a^2-\phi_z^2)\phi_{zz}-2\phi_x\phi_y\phi_{xy}$$
$$-2\phi_y\phi_z\phi_{yz}-2\phi_z\phi_x\phi_{zx}=0 \qquad (5)$$

Boundary Conditions

The computation region is a cylinder (Fig. 2) much larger than the inlet or body being analyzed. There is flow through all surfaces of the cylinder. On the left end and lower half of the cylinder, ϕ is specified with ϕ at the lower left point of the cylinder arbitrarily set to zero.

$$\phi=u_\infty r\cos\theta+w_\infty z+\phi_{\text{origin}} \qquad (6)$$

where ϕ_{origin} is determined so that $\phi=0$ at the lower left point of the cylinder. On the right end and upper half of the cylinder, ϕ_n (the velocity normal to the surface) is specified at the freestream value. On the upper half

$$\phi_n=-\phi_r=-u_\infty\cos\theta \qquad (7)$$

On the right end, except for the inlet duct-exit cross section,

$$\phi_n=-\phi_z=-w_\infty \qquad (8)$$

At the inlet duct exit, ϕ_n is specified to give the correct inlet mass flow (for inlet calculations). On the surfaces of the inlet and/or centerbody, ϕ_n is specified to be zero.

Only half of the field is computed, since there is a plane of symmetry for the axisymmetric body problem. The inlet or body is oriented so that $\theta=0°$ is the leeward side, $\theta=180°$ is the windward side, and, thus, the $y=0$ ($\theta=0°$, 180°) plane is the plane of symmetry. The analysis and computer program are also valid for negative angles of attack, which essentially have the effect of reversing the boundary conditions on the top and bottom of the cylinder.

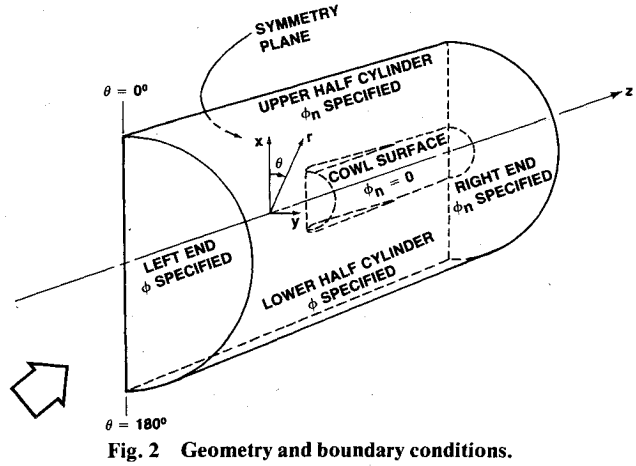

Fig. 2 Geometry and boundary conditions.

Point Types and Mesh Bookkeeping

The scheme used to keep track of the different types of mesh points near the surface and for keeping track of the surface-mesh line intersections is a straightforward extension of the one used previously. Full details are available in Ref. 1. In summary, the use of a Cartesian mesh leads to a variety of irregular mesh configurations at surfaces. Each type of computational mesh star requires a slightly different difference formula. Special weighted formulas are used if the distance from a mesh point to the surface is much smaller than the local mesh spacing. The complexity of the computer program is due to the number of special configurations, and the logic for switching between them, and for doing central or upwind differencing depending on the local Mach number. The differencing for any given type of surface-mesh intersection is relatively simple.

Finite-Difference Formulas

The difference quotients used to represent the partial derivatives are almost identical to those of Ref. 1. Central differencing is used when the flow is subsonic, and upwind differencing is used to handle supersonic flow. The procedure for switching from central to upwind differencing is described fully in Ref. 1. The major changes required are at the axis ($r=0$) and in the handling of θ derivatives. The finite-difference quotients for ϕ_r, ϕ_z, ϕ_{rr}, ϕ_{zz}, and ϕ_{rz}, except at the axis, are the same as Ref. 1. The original treatment of the derivatives with respect to θ was similar to the treatment of the z derivatives.

Finite-Difference Formulas at the Axis

On the plane of symmetry ($y=0$, $\theta=0°$ or 180°), the Cartesian mesh form of the potential Eq. (5) becomes

$$(a^2-\phi_z^2)\phi_{zz}+a^2\phi_{yy}+(a^2-\phi_x^2)\phi_{xx}-2\phi_z\phi_x\phi_{zx}=0 \quad (9)$$

This is the equation that is used along the axis. The ϕ_z and ϕ_{zz} difference quotients are computed the same as elsewhere in the field. Referring to Fig. 3 for notation, the special difference formulas at the axis for use in Eq. (9) are

$$\phi_x = \frac{\phi_{i,2,1}-\phi_{i,2,K}}{2\Delta r} \quad (10a)$$

$$\phi_{xx} = \frac{\phi_{i,2,1}-2\frac{1}{\omega_n}\phi_{i,1,1}{}^{+}-2\left(1-\frac{1}{\omega_n}\right)\phi_{i,1,1}+\phi_{i,2,K}{}^{+}}{\Delta r^2} \quad (10b)$$

$$\phi_{yy} = \frac{2\phi_{i,2,k90}-2\phi_{i,1,1}+}{\Delta r^2} \quad (10c)$$

The use of the over-relaxation parameter, ω_n, is discussed fully in Ref. 1. The + superscript indicates a value of ϕ being computed during the current relaxation sweep. The lack of the superscript indicates an old value of ϕ (already calculated on the previous sweep). The equation on the axis is solved only for $k=K(\theta=180°)$. This value then is held fixed as k is indexed from $K-1$ to 1. The cross derivative ϕ_{zx} is computed by differencing in z the formula for ϕ_x, Eq. (10a). The difference quotient used for the z derivative is the usual one. If the flow is supersonic, the upwind formula for ϕ_{zx} is straightforward. If $\phi_z>0$ and $\phi_x>0$, then

$$\phi_{zx_{\text{upwind}}} = \frac{\phi_{i,1,1}{}^{+}-\phi_{i-1,1,1}{}^{+}-\phi_{i,2,K}{}^{+}+\phi_{i-1,2,K}{}^{+}}{\Delta z_\ell \Delta r} \quad (11)$$

The switching between central and upwind differencing is handled the same as at any other mesh point.

If a body or centerbody is pointed, the point on the axis is a singularity in the flowfield. For the purposes of the computation, it is handled by making the surface point on the axis multivalued, with a different ϕ value for each θ mesh. This does not cause any computational problems, but the solution is not exact near the singularity. The boundary condition used at the tip is ϕ_n equals zero, which is differenced the same as at any other surface point. Since, at the tip, the normal to the surface $\boldsymbol{n}$ is undefined, a value of $\boldsymbol{n}$ is used just downstream along a $\theta=$ constant line.

Special θ Finite-Difference Quotients

When the initial computed results from the program were examined, it was discovered that u_θ was equal to a function of r and z times $\sin\theta$ to a better accuracy than the program results were expected to have. This implied that

$$\phi(r,\theta,z)=\phi_1(r,z)+\phi_2(r,z)r\cos\theta \quad (12)$$

where

$$u_r=\phi_r=\phi_{1_r}+(r\phi_2)_r\cos\theta \quad (13a)$$

$$u_\theta=\phi_\theta/r=-\phi_2\sin\theta \quad (13b)$$

$$w=\phi_z=\phi_{1_z}+r\phi_{2_z}\cos\theta \quad (13c)$$

After this behavior was observed, an explanation was sought because, if this behavior could be shown to occur in general, important time-saving changes in the program were possible. If Eq. (12) is substituted in Eq. (1) and it is assumed that the quantities $|u_\theta|/a$, $|(r\phi_2)_r|/a$, $|r\phi_{2_z}|/a$, $|(r\phi_2)_r|/(ar)$, and $|\phi_{2_z}|/a$ are all much smaller than one, and that the terms involving $\phi_{r\theta}$ and $\phi_{\theta z}$ are small relative to other terms and can be neglected, then the following equation is obtained:

$$\left(1-\frac{\phi_{1_r}^2}{a^2}\right)(\phi_{1_{rr}}+(r\phi_2)_{rr}\cos\theta)-\frac{\phi_2}{r}\cos\theta$$
$$+\left(1-\frac{\phi_{1_z}^2}{a^2}\right)(\phi_{1_{zz}}+r\phi_{2_{zz}}\cos\theta)-2\frac{\phi_{1_r}\phi_{1_z}}{a^2}$$
$$\times(\phi_{1_{rz}}+(r\phi_2)_{rz}\cos\theta)+\frac{\phi_{1_r}}{r}+\frac{(r\phi_2)_r}{r}\cos\theta=0 \quad (14)$$

These assumptions are essentially that $|u_\theta|/a$ is small and that its derivatives in r and z are also small. The foregoing equation is of the form

$$f(r,z)+g(r,z)\cos\theta=0 \quad (15)$$

Since θ is arbitrary, the only solution is that both $f(r,z)$ and $g(r,z)$ are equal to zero. The first equation that results is

$$\left(1-\frac{\phi_{1_r}^2}{a^2}\right)\phi_{1_{rr}}+\left(1-\frac{\phi_{1_z}^2}{a^2}\right)\phi_{1_{zz}}-2\frac{\phi_{1_r}\phi_{1_z}}{a^2}\phi_{1_{rz}}+\frac{\phi_{1_r}}{r}=0 \quad (16)$$

This can be recognized as the usual equation for axisymmetric potential flow. The second equation that is obtained is

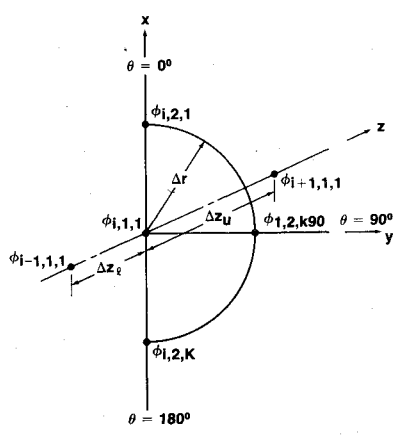

Fig. 3 Finite-difference mesh at the axis.

$$\left(1-\frac{\phi_{1_r}^2}{a^2}\right)(r\phi_2)_{rr}+\left(1-\frac{\phi_{1_z}^2}{a^2}\right)r\phi_{2_{zz}}$$

$$-2\frac{\phi_{1_r}\phi_{1_z}}{a^2}(r\phi_2)_{rz}+\phi_{2_r}=0 \tag{17}$$

Once Eq. (16) is solved for ϕ_1, the preceding equation is a linear second-order partial differential equation for ϕ_2. If Eq. (16) is solved with the freestream boundary condition $w=w_\infty$ and the given compressor-face mass flow, and Eq. (17) is solved with $(r\phi_2)_n$ equal to zero on the body surfaces, $(r\phi_2)_r$ equals u_∞ at the top of the flowfield, and ϕ_{2_z} equals zero at the right and left ends, then a solution of the form of Eq. (12) has been obtained. If the flow is incompressible the solution is exact. It is not unreasonable to assume that the derivatives of u_θ are well behaved, and that u_θ is of the order of u_∞. As an example for a 30-knot crosswind case, u_∞/a is approximately 0.05. Actually, near the hilite (forwardmost point on the cowl), for many of the results shown, it is questionable if all of the terms that are assumed small in the preceding argument are indeed small. The program does have the ability to compute with many θ planes. Typical cases have been computed using many θ planes and the results compared to the same calculations using five θ planes and the special θ differencing described next. No significant differences have been found when making these comparisons. This is a numerical verification that the solutions are of the form of Eq. (12) for surprisingly large values of some of the neglected terms. All of the results shown in this paper have been computed using the special θ difference quotients and only five θ planes (0, 45, 90, 135, and 180°), and the agreement with the experimental data is excellent.

When the program initially was written, the treatment of the θ derivatives was similar to the treatment of the z derivatives. After it was discovered that the solutions had the form of Eq. (12), a way was sought to take advantage of this behavior when it existed. The standard formula for the second-order difference quotient for ϕ_θ can be derived by writing

$$\phi_\theta=F_1\phi(\theta+\Delta\theta_u)+F_2\phi(\theta)+F_3\phi(\theta-\Delta\theta_\ell) \tag{18}$$

and using the trial function

$$\phi(\theta)=A+B\theta+C\theta^2 \tag{19}$$

to determine F_1, F_2, and F_3. This process results in the usual form of the difference quotient

$$\phi_\theta=\frac{\Delta\theta_\ell^2\phi(\theta+\Delta\theta_u)+(\Delta\theta_u^2-\Delta\theta_\ell^2)\phi(\theta)-\Delta\theta_u^2\phi(\theta-\Delta\theta_\ell)}{\Delta\theta_\ell\Delta\theta_u(\Delta\theta_\ell+\Delta\theta_u)} \tag{20}$$

If instead, the trial function

$$\phi(\theta)=A+B\cos\theta+C\sin\theta \tag{21}$$

is used, the following difference quotient is obtained:

$$\phi_\theta=[(1-\cos\Delta\theta_\ell)\phi(\theta+\Delta\theta_u)+(\cos\Delta\theta_\ell-\cos\Delta\theta_u)\phi(\theta)$$
$$-(1-\cos\Delta\theta_u)\phi(\theta-\Delta\theta_\ell)]/[\sin\Delta\theta_u+\sin\Delta\theta_\ell$$
$$-\sin(\Delta\theta_\ell+\Delta\theta_u)] \tag{22}$$

The two formulas for ϕ_θ are equivalent to order $\Delta\theta^2$, but when $\phi(\theta)\approx A+B\cos\theta$, which is the situation here, Eq. (22) gives very high accuracy even when $\Delta\theta=90°$.

The following formula for $\phi_{\theta\theta}$ is obtained using the same approach:

$$\phi_{\theta\theta}=$$
$$\frac{\sin\Delta\theta_\ell\phi(\theta+\Delta\theta_u)-(\sin\Delta\theta_\ell+\sin\Delta\theta_u)\phi(\theta)+\sin\Delta\theta_u\phi(\theta-\Delta\theta_\ell)}{\sin\Delta\theta_\ell+\sin\Delta\theta_u-\sin(\Delta\theta_\ell+\Delta\theta_u)} \tag{23}$$

This formula actually is used with a local over-relaxation parameter ω, which is calculated in the same manner as in the ϕ_{zz} differencing (see Ref. 1). The formula then becomes

$$\phi_{\theta\theta}=\left\{\sin\Delta\theta_\ell\phi_{i,j,k+1}{}^{+}-(\sin\Delta\theta_\ell+\sin\Delta\theta_u)\left[\frac{1}{\omega}\phi_{i,j,k}{}^{+}\right.\right.$$
$$\left.\left.+\left(1-\frac{1}{\omega}\right)\phi_{i,j,k}\right]+\sin\Delta\theta_u\phi_{i,j,k-1}\right\}$$
$$\div\left[\sin\Delta\theta_\ell+\sin\Delta\theta_u-\sin(\Delta\theta_\ell+\Delta\theta_u)\right] \tag{24}$$

No provision has been made for supersonic crossflow velocities, although the extension would be straightforward. If the flow is supersonic, upwind $\phi_{r\theta}$ and $\phi_{z\theta}$ derivatives are calculated in the obvious manner.

The present version of the computer program has the special forms for ϕ_θ and $\phi_{\theta\theta}$. However, they are equivalent, to second order, to the usual difference quotients. Thus, by using many θ=constant planes for a computation, the program can solve for flows where $|u_\theta|/a$ is not small.

Plane of Symmetry

At the plane of symmetry ($\theta=0°$ or 180°), Eq. (1) becomes

$$(a^2-\phi_r^2)\phi_{rr}+\frac{a^2}{r^2}\phi_{\theta\theta}+(a^2-\phi_z^2)\phi_{zz}-2\phi_r\phi_z\phi_{rz}+\frac{a^2}{r}\phi_r=0 \tag{25}$$

The r and z derivatives are handled in standard fashion. The difference quotient for $\phi_{\theta\theta}$ is computed using symmetry. For the $k=1$ ($\theta=0°$) plane

$$\phi_{\theta\theta}=\frac{\phi_{i,j,2}{}^{+}-\phi_{i,j,1}{}^{+}}{1-\cos\Delta\theta} \tag{26}$$

Body Surface Boundary Condition

The body surface boundary condition, $\phi_n=\partial\phi/\partial n=0$, is handled the same as in Ref. 1. There is no contribution from u_θ since the restriction that the body geometry is axisymmetric insures that u_θ does not contribute to ϕ_n.

Upper-Far-Boundary Boundary Condition

The boundary condition on the upper half of the cylinder (see Fig. 2) and the right end of the computational domain is that ϕ_n is specified: $\phi_n=-\phi_r$ on the upper half of the cylinder, and $\phi_n=-\phi_z$ on the right end. The standard three-point backward-difference formula is used on the upper half of the cylinder, and a two-point backward-difference formula is used at the right end.

Initial Field

The calculation is started by initializing the flowfield so that, inside the inlet duct, the ϕ field is set for the correct mass flow one dimensionally [$\phi_{\text{initial}}=\phi(z)$ inside the duct]. Far outside the duct, the initial flowfield is set to the velocity at infinity. In the vicinity of the inlet entrance there is a smooth fairing between the ϕ distribution inside the inlet and that far from the inlet. The initial field, in general, has a discontinuity in the flowfield at the inlet entrance and has flow through surfaces. The calculation is started at a very low Mach number and is brought gradually to the correct Mach number by sweep 15. This allows the local flow to become aligned with adjacent surfaces before any of the upwind differencing is used. The calculation is run from the beginning with the same over-relaxation parameters.

Line Relaxation and Relaxation Procedure

Line relaxation is used along radial lines (z and θ=constant). Lines start at either the axis or a surface and end at the far boundary or on another surface, depending on the

configuration. Surface points adjacent to mesh points on the line are solved simultaneously with the line. The sweeping from line to line is done from $\theta = 180°$ to $\theta = 0°$ for constant z, before the next z = constant plane is processed. Sweeping is in the direction of increasing z. This means that the sweep direction is in the prevailing flow direction.

Solution Procedure

The solution procedure is identical to that of Ref. 1 with the addition of sweeping in the θ direction. This includes initial convergence of the field on a coarse mesh and extrapolation of residue fields which is described fully in Ref. 1. The computation is run from the beginning with the over-relaxation parameter ω_n equal to 1.85. The use of a coarse mesh for initial convergence is even more advantageous for three dimensions, since there are only approximately ⅛ as many points in the coarse mesh. This factor of ⅛, in combination with the doubling in the convergence rate per sweep normally experienced with a coarse mesh, gives a factor of 16 computation-time advantage to using the coarse mesh for the initial part of the relaxation process.

Computation Parameters

The analysis is programmed in FORTRAN IV for the CDC 6600 computer. The program requires 115,000 octal words of core storage and also uses disk storage. This program storage requirement has been obtained by using an overlay structure for the program and by using disk storage to store parts of the ϕ field while other parts are being calculated. A standard inlet computation takes 200 coarse mesh sweeps and 150 fine mesh sweeps. At the end of the computation the maximum residue ($\Delta\phi$ change between successive sweeps at a mesh point) is typically smaller than or equal to 10^{-5} when ϕ is scaled so that the maximum ϕ value in the field is approximately one. At this point the solution normally is converged to better than ± 0.02 in Mach number, which is roughly the overall order of accuracy that can be expected with the typical mesh spacings used. On a standard run, five fine mesh θ = constant planes, a maximum of 70 z = constant planes, and 40 r = constant surfaces are used. The run time using OPT = 1 or 2 for the FTN compiler is on the order of 12 to 15 min, depending on geometry, number of calculation points, number of supersonic points in the field, etc. The time per sweep is on the order of 0.6 to 0.8 sec in the coarse mesh (20 by 3 by 30) and 4 to 5 sec in the fine mesh. Times using the RUN compiler are 50% longer. Accuracy using these meshes is discussed under Results.

Results

Figures 4-7 show comparisons between theory and experiment for two 51-cm-diam inlets tested[11] in the NASA Lewis Research Center 9- by 15-ft V/STOL propulsion wind tunnel. One inlet had a 1.35 contraction ratio (area of inlet hilite/area of inlet throat), and the other inlet had a 1.26 contraction ratio. Comparisons are shown at two different airflows for each inlet. Agreement with experiment is very good.

There are probably two primary causes of the minor disagreement shown between the analysis and the experiment. The first is the effect of the inlet boundary layer. The places where boundary-layer effects are important are in the diffuser, where the boundary layer has a blockage effect that causes the measured Mach number to be higher than the potential flow value, and at shocks, where there can be significant effects on the inlet surface pressure distribution due to shock-wave/boundary-layer interaction. The second main cause of disagreement would be inaccuracy in the solution of the potential equation. There are possible problems with accuracy where flow gradients are very strong, since the program uses a finite mesh size. There also may be problems at shocks since this analysis uses nonconservative differencing, and it has been shown[12,13] that this can cause errors in the vicinity of shocks. The errors due to the use of

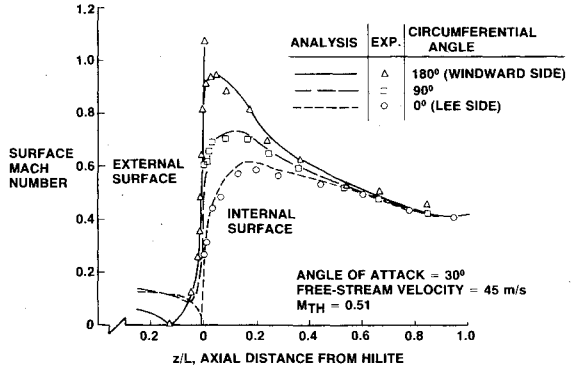

Fig. 4 Cowl surface Mach number distribution for 1.35 contraction ratio inlet.

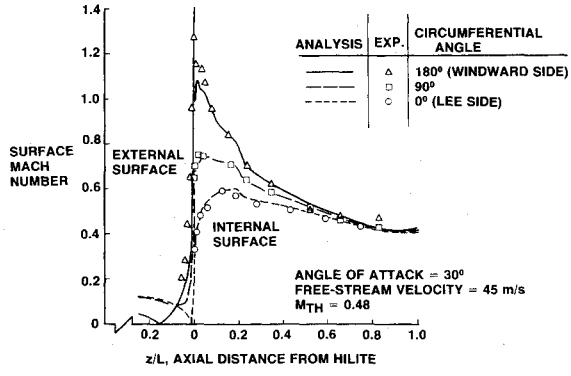

Fig. 6 Cowl surface Mach number distribution for 1.26 contraction ratio inlet.

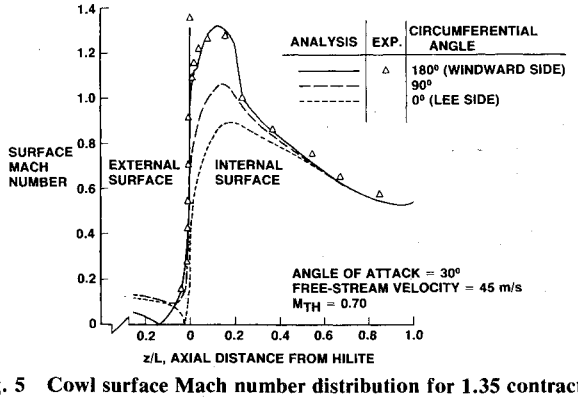

Fig. 5 Cowl surface Mach number distribution for 1.35 contraction ratio inlet.

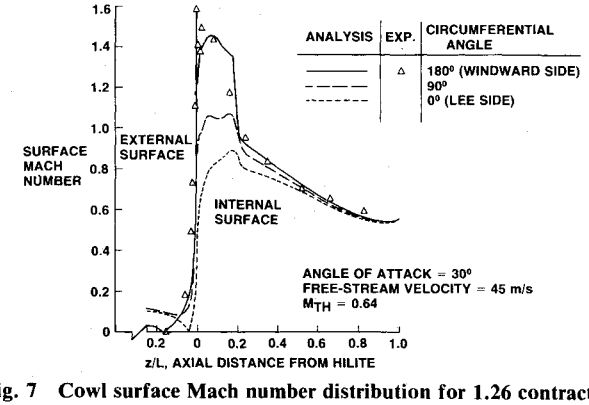

Fig. 7 Cowl surface Mach number distribution for 1.26 contraction ratio inlet.

nonconservative differencing and the errors due to neglect of the inlet boundary layer tend to be compensating, and this may account partially for the excellent agreement with data. A minor source of error is that the data were taken from small figures in the original report.

Both inlets at this angle of attack have shocks and very strong flow gradients at the hilite where there is a Mach number spike detected by the analysis, even though it is spread over only one or two mesh spacings. The experimental results indicate that this Mach number spike is a real phenomena, although it is questionable if the analysis is predicting its magnitude accurately. The Mach number spike probably is caused by the rapid change in the radius of curvature of the surface in the vicinity of the hilite and would be affected by the inlet boundary layer.

The results for the previous two inlets and the results that follow all are calculated using a calculation cylinder with a diameter approximately five times the diameter of the inlet and extending approximately two and one-half inlet diameters ahead of the inlet. These are thought to be reasonable numbers, since, in practice, the inlets are tested in wind tunnels of finite size and used on aircraft where the flowfield about the inlet is affected by the wing and the fuselage. Thus, the results to which the analysis is being compared and the uses for which the analysis is developed are not an inlet in an infinite field, and it is not possible by comparing with the data to correctly determine the effects of using different-size computational regions. Neither will these effects help determine the behavior of the installed inlet.

Figures 8-11 show comparisons between the analysis and experiment[14] for a 13.97-cm-diam, 1.30 contraction ratio, translating-centerbody inlet at STOL operating conditions. The results for angles of attack of 20° and 40°, for the centerbody both retracted and extended, illustrate the excellent agreement obtained between the analysis and the experiment.

Figure 12 shows a comparison between theory and experiment[15] for a high throat Mach number inlet for the quiet, clean, short-haul experimental engine (QCSEE). A comparison is shown for entry lip 3, which has a 1.56 contraction ratio and a diffuser-exit diameter of 30.48 cm. The test was conducted in the NASA Lewis 9- by 15 ft V/STOL wind tunnel. The case shown is one for which the inlet was choked, and there is a strong shock with significant normal shock-wave/boundary-layer interaction effects at the throat. It is probably a very thick boundary layer which causes the disagreement between the analysis and experiment downstream of the throat. Agreement is not perfect for the windward (180°) side at the hilite, where there is a shock and strong gradients that effect the accuracy.

The inlets for which comparisons have been made are shown in cross section in Fig. 13.

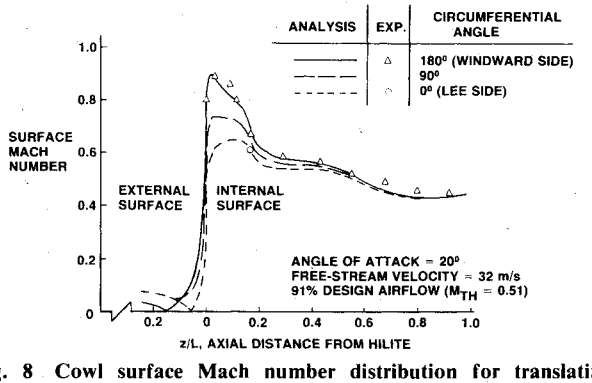

Fig. 8 Cowl surface Mach number distribution for translating centerbody inlet, centerbody retracted.

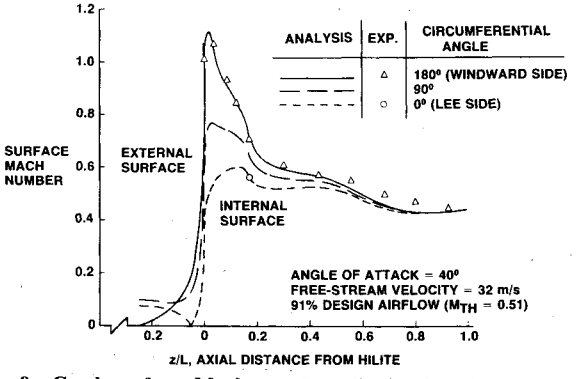

Fig. 9 Cowl surface Mach number distribution for translating centerbody inlet, centerbody retracted.

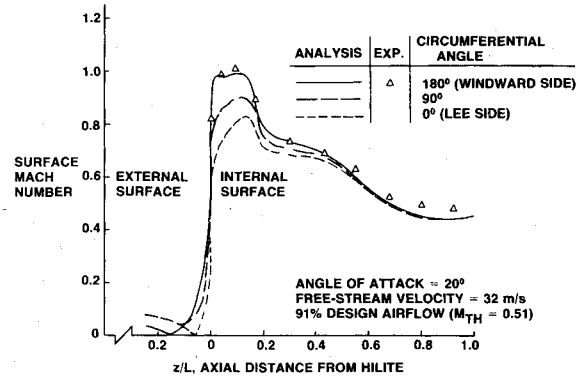

Fig. 10 Cowl surface Mach number distribution for translating centerbody inlet, centerbody extended.

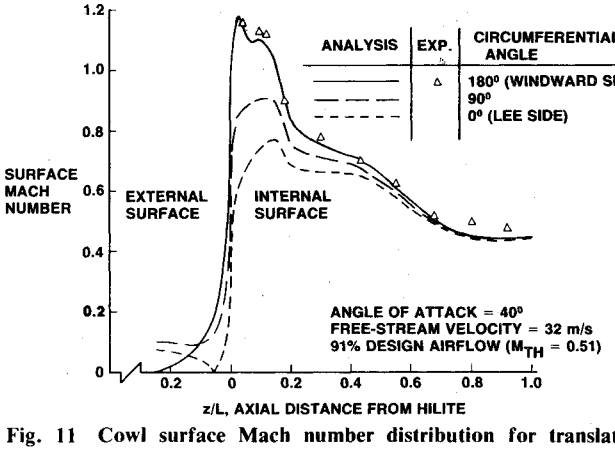

Fig. 11 Cowl surface Mach number distribution for translating centerbody inlet, centerbody extended.

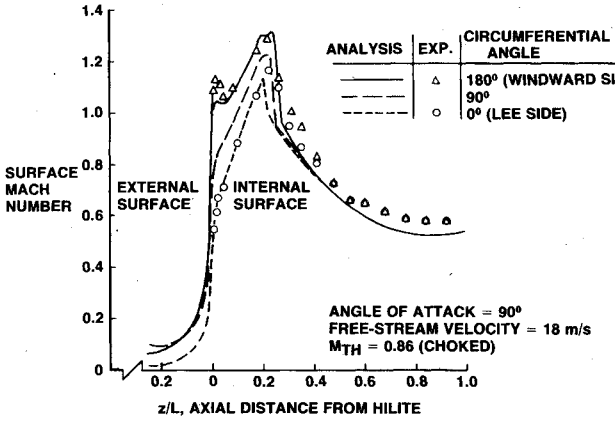

Fig. 12 Cowl surface Mach number distribution for high throat Mach number QCSEE inlet.

The preceding results have been for inlets at low speeds and large angles of attack. Results are shown in Ref. 1 for inlets at high forward speeds at zero angle of attack. Although results are not shown for high subsonic speeds and small angles of attack, the analysis should predict such flowfields correctly. The following results show the programs ability to predict external flows at high subsonic Mach numbers.

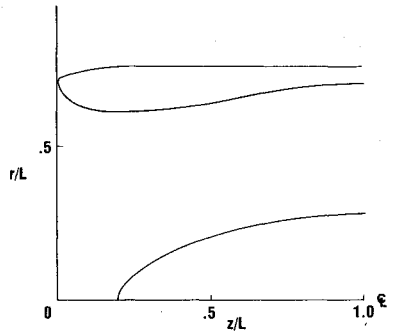

a) 1.35 contraction ratio inlet.

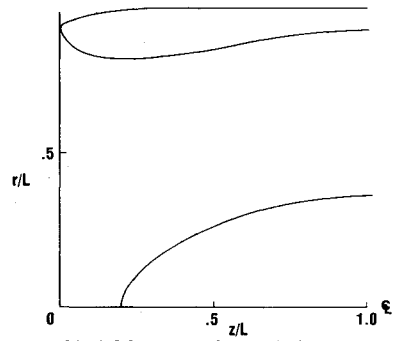

b) 1.26 contraction ratio inlet.

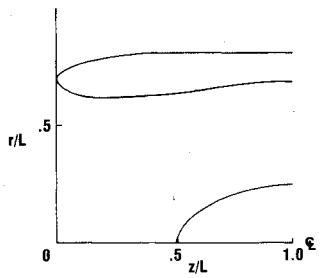

c) Translating centerbody inlet, centerbody retracted.

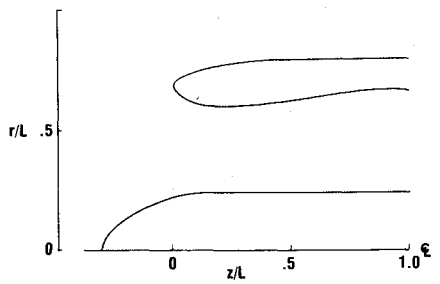

d) Translating centerbody inlet, centerbody extended.

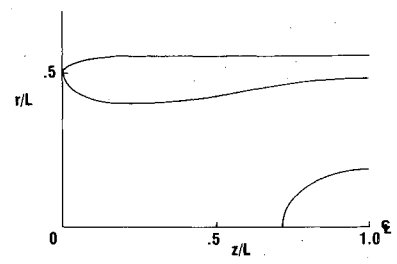

e) High throat Mach number QCSEE inlet.

Fig. 13 Cross sections of inlets analyzed.

Figures 14 and 15 show comparisons between the analysis and experiment[16] for an axisymmetric body (shown in cross section in Fig. 14) at 10.23° and 20.24° angles of attack at $M_\infty = 0.83$. The body is configuration 5 of the reference and has a maximum diameter D of 14.605 cm. It was tested in the NASA-Langley high-speed 7×10ft tunnel. These figures show the program's capability to provide good results where local Mach numbers are quite high. Disagreement downstream of $z/D \approx 3.05$ is caused by the actual body having a rearward-facing step at $z/D = 3.5$, resulting in a base-flow problem which is beyond the scope of this analysis. There are probably also boundary-layer effects because of the shock at $z/D = 3.0$, particularly at the higher angle of attack. The computational region extended 10-diam ahead of and behind the body and had a diameter 40 times the body diameter.

Comments on Accuracy

The mesh used, which had up to 70 z = constant planes and 40 r = constant surfaces, is certainly adequate as shown previously. Results for the coarse mesh (30 by 20) are very poor in comparison. The fine mesh used is a good compromise between cost and accuracy, but experimentation with different meshes for several of the data cases has indicated that the results for some of the regions where the flow gradients are quite large are slightly dependent on the mesh chosen. If necessary, the problem of large gradients could be resolved by the use of denser meshes. The results of the analysis are quite adequate if the mesh locations are chosen with reasonable care. As a specific example of program accuracy with typical meshes, the conservation of mass along the inlet duct is typically on the order of 1% or 2% from the hilite to the duct exit.

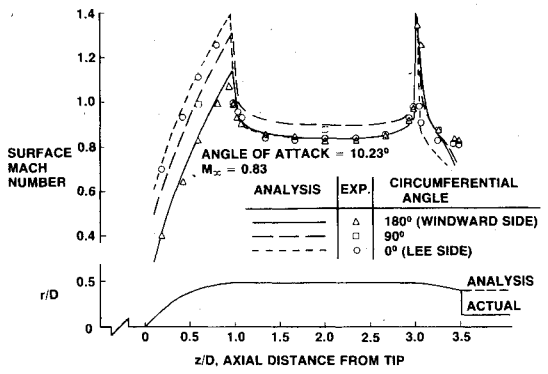

Fig. 14 Surface Mach number distribution for and geometry of axisymmetric body.

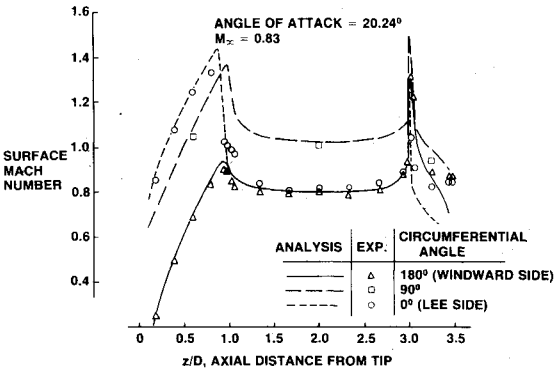

Fig. 15 Surface Mach number distribution for axisymmetric body.

Conclusions

The analysis has been shown to give very good agreement with experiment. For most cases of interest $|u_\theta|/a$ is sufficiently small that $u_\theta \approx -\phi_2(r,z)\sin\theta$. Taking advantage of this behavior leads to greatly reduced computational cost. Because of its accuracy and reasonable cost, this analysis has proven to be an extremely useful inlet analysis and design tool.

The basic analysis ideas are not restricted to axisymmetric inlets. An extension to general inlet shapes would be lengthy but would not involve much technical risk. The most severe problem may be that there no longer is a plane of symmetry, and u_θ no longer would behave as $\sin\theta$; thus many more mesh points would be required to obtain a solution with attendant severe increase in computational costs.

Acknowledgment

The authors wishes to acknowledge the assistance of R.G. Jorstad of Boeing Computer Services, Inc., who was responsible for the programming of the analysis.

References

[1] Reyhner, T.A., "Cartesian Mesh Solution for Axisymmetric Transonic Potential Flow Around Inlets," *AIAA Journal,* Vol. 15, May 1977, pp. 624-631.

[2] Magnus, R. and Yoshihara, H., "Inviscid Transonic Flow Over Airfoils," *AIAA Journal,* Vol, 8, Dec. 1970, pp. 2157-2162.

[3] Carlson, L.A., "Transonic Airfoil Analysis and Design Using Cartesian Coordinates," *Journal of Aircraft,* Vol. 13, May 1976, pp. 349-356.

[4] Arlinger, B.G., "Calculation of Transonic Flow Around Axisymmetric Inlets," *AIAA Journal,* Vol. 13, Dec. 1975, pp. 1614-1621.

[5] Colehour, J.L., "Transonic Flow Analysis Using a Streamline Coordinate Transformation Procedure," AIAA Paper 73-657, July 1973, Palm Springs, Calif.

[6] Caughey, D.A. and Jameson, A., "Accelerated Iterative Calculation of Transonic Nacelle Flowfields," AIAA Paper 76-100, Jan. 1976, Washington, D.C.

[7] South, J.C. and Jameson, A., "Relaxation Solutions for Inviscid Axisymmetric Transonic Flow Over Blunt or Pointed Bodies," *Proceedings AIAA Computational Fluid Dynamics Conference,* Palm Springs, Calif., July 1973, pp. 8-17.

[8] Ives, D.C. and Liutermoza, J.F., "Analysis of Transonic Cascade Flow Using Conformal Mapping and Relaxation Techniques," *AIAA Journal,* Vol. 15, May 1977, pp. 647-652.

[9] Jameson, A., "Numerical Calculation of the Three-Dimensional Transonic Flow Over a Yawed Wing," *Proceedings AIAA Computational Fluid Dynamics Conference,* Palm Springs, Calif., July 1973, pp. 18-26.

[10] Jameson, A., "Iterative Solution of Transonic Flows Over Airfoils and Wings, Including Flows at Mach 1," *Communications on Pure and Applied Mathematics,* Vol. 27, May 1974, pp. 283-309.

[11] Albers, J.A., "Comparison of Predicted and Measured Low-Speed Performance of Two 51-Centimeter-Diameter Inlets at Incidence Angle," NASA TM X-2937, 1973.

[12] Murman, E.M., "Analysis of Embedded Shock Waves Calculated by Relaxation Methods," *AIAA Journal,* Vol. 12, May 1974, pp. 626-633.

[13] Jameson, A., "Transonic Potential Flow Calculations Using Conservation Form," *Proceedings of the AIAA 2nd Computational Fluid Dynamics Conference,* Hartford, Conn., June 19-20, 1975, pp. 148-155.

[14] Albers, J.A., "Theoretical and Experimental Internal Flow Characteristics of a 13.97-Centimeter-Diameter Inlet at STOL Takeoff and Approach Conditions," NASA TN D-7185, 1973.

[15] Miller, B.A., Dastoli, B.J., and Wesoky, H.L., "Effect of Entry-Lip Design on Aerodynamics and Acoustics of High Throat Mach Number Inlets for the Quiet, Clean, Short-Haul Experimental Engine," NASA TM X-3222, 1975.

[16] Fox, C.H., Jr., "Experimental Surface Pressure Distributions for a Family of Axisymmetric Bodies at Subsonic Speeds," NASA TM X-2439, 1971.